

Quantification of the Knudsen Effect on the Effective Gas Diffusion Coefficient in Partially Saturated Pore Distributions


Christoph Strangfeld

The effective gas diffusion coefficient describes the process of gas diffusion in porous materials. Several materials have a significant number of micropores in the lower nanometre range leading to a reduction of gas diffusion (Knudsen effect). In the case of partial pore saturation during adsorption, the available pore space is further reduced, as is the gas diffusion. In this study, the influence of partially saturated pores on the Knudsen effect and on the gas diffusion is quantified. Three different pore geometries are investigated (slit, cylindrical and spherical pores) and three different types of pore size distribution, including a broad equal distribution, three narrow normal distributions and two measured distributions of concrete. Besides the intensive computation of the exact pore saturation, a simplified model with low computational requirements is suggested. This study shows that the influence of the water layer thickness on the effective diffusion becomes significant for pore radii below 50 nm and the assumed pore geometry is important. At the end, the overall effect is quantified for an amorphous material with most pore radii below 30 nm. At a moisture level of 50% relative humidity, the effective diffusion is reduced by 35% due to partial saturation.

1. Introduction

Diffusion is the gradual compensation of concentration differences without external forces. This natural process is driven by Brownian motion and occurs in all materials: gases, liquids, and solids. In porous materials, diffusion takes place in the open porosity of the material. In the case of very fine pores, Knudsen diffusion reduces the ordinary molecular diffusion. Knudsen diffusion is important in chemical processes such as catalysis, filtration, and separation processes^[1–3] and determines the performance of proton exchange membranes in fuel cells.^[4]

Dr. C. Strangfeld
Non-Destructive Testing
Non-Destructive Testing Methods for Civil Engineering
Bundesanstalt für Materialforschung und -prüfung
Unter den Eichen 87, Berlin 12205, Germany
E-mail: christoph.strangfeld@bam.de

 The ORCID identification number(s) for the author(s) of this article can be found under <https://doi.org/10.1002/adem.202100106>.

© 2021 The Authors. Advanced Engineering Materials published by Wiley-VCH GmbH. This is an open access article under the terms of the Creative Commons Attribution License, which permits use, distribution and reproduction in any medium, provided the original work is properly cited.

DOI: 10.1002/adem.202100106

In environmental science, it is important for seawater desalination^[5] and governs the natural migration of radon gas from certain earth crust materials.^[6] In material science, Knudsen diffusion is crucial for breathable and protective fabrics based on carbon nanotubes^[7] and essential for microporous membranes to clean-energy technologies.^[8] Furthermore, it has a significant influence on the service life of structures in civil engineering.^[9]

In general, ions migrate into a porous material through the adsorbed substance, e.g., water, in the pore system. Thus, these processes greatly depend on the amount of adsorbed substance, e.g., the material's moisture content. In contrast, gases are transported in the open space within the pore system. In the case of an amorphous material, the pore system is very complex. Thus, the relationship between the effective gas diffusion coefficient and the porosity is strongly nonlinear.^[10] Considering for

instance hydraulically bound materials, the pore sizes vary over several magnitudes from a few nanometers to several micrometers and a large proportion of the pore volume consists of pores with radii below 100 nm.^[11,12] Pore shape, tortuosity, and the orientation of pore connections must be considered in diffusion processes.^[13–15] Depending on the pore size and the moisture content, gas diffusion occurs by different diffusion mechanisms. In large pores in the range of micrometers, molecular diffusion dominates the gas transport. In this state, the pore space is much greater than the mean free path length of a molecule. The entire process can be described by molecule–molecule collisions and has one diffusion coefficient for the entire gas mixture.^[13] In small pores in the range of nanometers, Knudsen diffusion sets in because the mean free path length of a molecule is much greater than the limited pore space. In this case, molecule–pore wall collisions dominate.^[13] Molecular diffusion is therefore significantly reduced by the Knudsen effect.^[16,17] At very low moisture contents or in dry material, surface diffusion might occur or dominate in tiny pores.^[16] However, in this study, partially saturated pores are investigated and so, surface diffusion plays only a negligible role.^[14]

In porous materials with pores in the nanometre range, molecular and Knudsen diffusion coexist and it is essential to consider both effects.^[10,13,17–20] The transient state starts approximately when pore radii are below ≈ 30 –200 nm and

ends at around 2 nm.^[6,14,18,21,22] Thus, the effective gas diffusion is a nonlinear function of these two effects and depends on the pore system being investigated. Empirical models that correlate porosity and gas diffusion cannot therefore be applied due to the high complexity of this process.^[16] Furthermore, a simple analytical consideration based on Fick's law generally fails because it is valid only for molecular diffusion.^[6,16,23] To take this issue into account, some authors have incorporated the limited space of dry pores and calculated the Knudsen effect for the given pore system.^[20,24,25] However, this does not take the influence of pore saturation on the Knudsen effect into account.

If more substance is adsorbed, the saturation of the porous material increases. For instance, the water layer thickness in the pores will increase during water vapor adsorption.^[26] This reduces the available free space or leads to the full saturation of small pores.^[6,27,28] The Knudsen effect is then increased and reduces the effective gas diffusion significantly.^[21,29] In addition, swelling of the material due to interlayer water further reduces the free space for molecular diffusion.^[26] In cement-based materials, gas diffusion coefficients at dry state of $10^{-6} \text{ m}^2 \text{ s}^{-1}$ are reduced to $10^{-13} \text{ m}^2 \text{ s}^{-1}$ at high saturation levels above 80%.^[13,30] Odeh et al. computed the effective pore radius due to water adsorption and its effect on Knudsen diffusion. However, only the average pore radius of the concrete was used, and the pore distribution was not considered.^[6] Some authors have investigated small samples of a few centimeters and incorporated the entire pore distribution and its varying water layer thickness during adsorption. They concluded that pore saturation significantly influences the predicted effective gas diffusion and that this issue should therefore receive greater attention.^[21,31,32] Similar effects are also known from modeling flow physics in soils.^[33,34] Several studies showed that the effective gas diffusion coefficient is significantly reduced due to the Knudsen effect at pore diameter below $1 \mu\text{m}$.^[35,36] As before, adsorption of water reduces the pore space as well as the effective gas diffusion.^[35–37] To incorporate both, molecular and Knudsen diffusion, the so-called dusty gas model is often used.^[38] Based on this model, a reduction of the effective gas diffusion of several orders of magnitude is predicted for different soils at dry state or high saturation of 80%.^[39] Although this model requires several, often unknown, parameters, it shows sufficient accuracy for many gases. In addition to other assumptions in this model, the diffusion coefficient is the reciprocal of linear combination of the gas–gas and gas–wall collision resistance.^[36,38] For the prediction of moisture flux, this assumption is highly questionable.

Numerical simulations of porous media quite frequently require a computation of diffusion coefficients, especially because problems including adsorption, temperature gradients, pore structure evolution, etc. are nonlinear. However, the modeling of the different effects and their interaction are not completely understood so far. For instance, modeling flow in unsaturated soils still reveals physical inconsistencies, which need to be eliminated.^[40] For long-term prediction of structures made of concrete, the different flow physics and their interaction with each other in the porous cement matrix is still an open research field.^[41] If nanopores are considered, models limited to molecular diffusion are insufficient and Knudsen effects must be included.^[42] For nondry materials, the water layer thickness needs to be predicted as well for the entire pore system.^[43] Although Maekawa et al. were aware of this important issue during calculations of concrete's performance, they calculated the water layer thickness only for the average pore radius due to the high computational costs involved.^[44]

In this study, the Knudsen number of partially saturated pore distributions is calculated. Three different pore geometries are investigated: slit, cylindrical, and spherical pores. Water vapor adsorption is considered and Hillerborg's adsorption theory is used to compute the corresponding water layer thickness.^[45] Hillerborg's approach of predicting the adsorbed water already incorporates the Kelvin equation, i.e., the pore curvature. Thus, the artificial differentiation between water film moisture and capillary moisture is obsolete. Both occur simultaneously and are computed in one step.^[45] Furthermore, different pore size distributions are investigated. These include theoretical equal and normal distributions as well as the real pore distribution of an ultrahigh-performance concrete (UHPC). Based on this, the reduction of effective gas diffusion due to the Knudsen effect of partially saturated pores is quantified for the entire sorption isotherm. Furthermore, a simplified model, which shows good correlation to the full model and requires only negligible computational costs, is discussed.

2. Theory

In partially saturated pores, the effective gas diffusion is a combination of molecular and Knudsen diffusion.^[10,13,17,18,20] Their respective contributions depend on the pore volume distribution and the pore saturation. **Figure 1** shows the different diffusion states and the effect of pore saturation. In Figure 1a, only

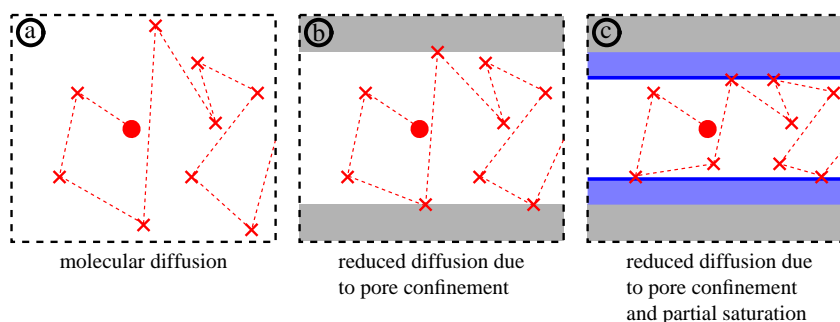


Figure 1. Diffusion in free and confined space; gray: cement matrix; blue: water layer.

pure molecular diffusion occurs. The molecule (red dot) travels through the unconfined space and collides only with other molecules (red crosses). This consideration is valid in atmospheric air or in large pores, i.e., $r > 1 \mu\text{m}$. If no confinement exists, the effective gas diffusion is equal to the molecular diffusion. Figure 1b shows the transient state. The molecule collides with other molecules as well as with the pore fringe. In this case, the effective gas diffusion is already significantly reduced by the Knudsen effect. If the material adsorbs water, a water layer of a few nanometers will form at the pore fringes. This would reduce the limited space further, especially in small pores with $r < 50 \text{ nm}$. The molecule would then collide more often with the pore fringe, or rather, the surface of the water layer. In the following, the diffusion of water vapor in porous materials is considered.

$$q_v = -\frac{\rho_{v,\text{sat}}\phi D_0}{\Omega} \int_{r_{\text{min}}}^{r_{\text{max}}} \frac{dV}{1 + N_k} \nabla h \quad (1)$$

If the moisture transport in the gas phase in porous materials is to be calculated, the reduction of the effective gas diffusion due to the Knudsen effect must be considered. This is shown in Equation (1).^[41] Here, q_v in $\text{kg m}^{-2} \text{s}^{-1}$ is the water vapor flux, $\rho_{v,\text{sat}}$ in kg m^{-3} is the saturated water vapour density, ϕ is the open porosity, D_0 in $\text{m}^2 \text{s}^{-1}$ is the water vapor diffusion coefficient in free atmosphere, and Ω describes the tortuosity of the pore system. These parameters in front of the integral in Equation (1) describe the molecular diffusion, and the integral accounts for the Knudsen effect. If the Knudsen number is $N_k \ll 1$, the integral reaches its maximum value of 1 and the effective gas diffusion is equal to the molecular diffusion. In contrast, if N_k is significantly above zero, the effective gas diffusion is reduced by the Knudsen effect. The integral starts at r_{min} in meters, which represents the radius of the smallest partially saturated pore, and r_{max} in meters is the largest pore in the pore system being investigated. V is the normalized pore volume of the radius being considered and h is the relative humidity.

$$N_k = \frac{l_m}{2(r - t_a)} \quad (2)$$

The Knudsen number is the mean free path of a gas l_m in meters divided by the effective pore space.^[31,41] In a partially saturated state, the pore radius r in meters and the adsorbed water layer thickness t_a in meters will both depend on the pore geometry. This is shown in **Figure 2** for a slit pore, a cylindrical pore, and a spherical pore. Slit pore geometry is defined as two infinite parallel plates which form the corresponding pore volume. The so-called pore radius is half the distance between the two parallel

pore walls. Thus, the water layer has no curvature and the pore saturation is independent of the pore size.^[46] In contrast, the curvature of a cylindrical or a spherical pore varies. The smaller the pore, the smaller is the radius of the water layer, which increases both the water adsorption and pore saturation. This phenomenon is shown in Equation (3) and (4), which incorporate the Kelvin equation.^[47]

$$t_a = \frac{t_w h C}{\left(1 - \frac{h}{h_m}\right)\left(1 - \frac{h}{h_m} + Ch\right)} \quad (3)$$

$$h_m = \exp\left(-\frac{\gamma M}{\rho_l RT} \left(\frac{1}{r_1 - t_a} + \frac{1}{r_2 - t_a}\right)\right) \quad (4)$$

C is a material constant related to the heat of adsorption in the first layer.^[46] t_w in meters is the thickness of one monomolecular water layer. R in $\text{J mol}^{-1} \text{K}^{-1}$ is the ideal gas constant, T in kelvin the temperature, M in kg mol^{-1} the molecular mass of water, and γ in N m^{-1} is the surface tension of liquid water. During adsorption, the humidity at which the air volume in the centre of a pore disappears is the so-called maximum humidity h_m . In fact, the smaller the two radii r_1 and r_2 in two perpendicular directions, the higher is the pore saturation.^[45,48] Thereby, adsorbed water already incorporates water film moisture and capillary moisture and therefore, Hillerborgs approach is able to predict the material moisture for the entire sorption isotherm. Equation (5)–(7) give the saturation depending on the pore geometry.

$$S_{\text{slit}} = \frac{t_a}{r} \quad (5)$$

$$S_{\text{cylindrical}} = 1 - \left(\frac{r - t_a}{r}\right)^2 \quad (6)$$

$$S_{\text{spherical}} = 1 - \left(\frac{r - t_a}{r}\right)^3 \quad (7)$$

As shown in Figure 2, the pore size and the assumed pore geometry influence the pore saturation. Thus, the Knudsen effect and its influence on the effective gas diffusion is also a function of pore geometry. At a given humidity, a spherical pore will always hold a thicker water layer than a cylindrical or slit pore. The smaller the pore, the more significant the Knudsen effect will be. The Knudsen number can thereby vary between zero and infinity. For a better comparison, the Knudsen quotient Q_K is considered for every pore radii in the following. The range of Q_K is between 0 and 1 and thus directly quantifies the reduction in molecular diffusion that is due to the Knudsen effect for one pore size.

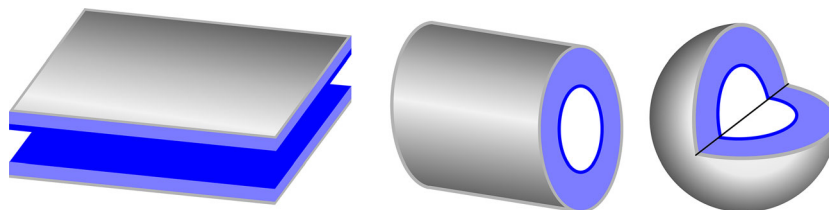


Figure 2. Illustration of a partially saturated slit, cylindrical, and spherical pore.

$$Q_K = \frac{1}{(1 + N_K)} \quad (8)$$

Furthermore, the normalized effective gas diffusion $D_{\text{eff, norm}}$ is considered for the different humidity levels. $D_{\text{eff, norm}}$ depends only on the pore volume distribution and the humidity and therefore directly quantifies the reduction of molecular diffusion due to the Knudsen effect for the entire pore size distribution. Its range is between 0 and 1.

$$D_{\text{eff, norm}} = \frac{D_{\text{eff}}}{D_0} = \int_{r_{\text{min}}}^{r_{\text{max}}} Q_K dV \quad (9)$$

For clarity, the collisions of water vapor molecules are assumed as fully elastic without any interaction with the pore fringe or the water layer at the pore fringe. Consequently, all gas collisions are equivalent and no phase transition with the liquid phase is assumed to occur.

3. Pore Saturation and Pore Size Distributions

First, the pore saturation is discussed. The thickness of the water layer depends on the pore radius, the pore geometry, and the relative humidity. Based on this knowledge, the remaining free space in the pore can be calculated to determine the Knudsen number. In a second step, this approach for one pore should then be applicable for a pore size distribution. The three theoretical pore distributions also are introduced, and the required material parameters are presented briefly.

3.1. The Influence of Pore Geometry on Pore Saturation

As discussed, pore saturation is a function of the pore radius and the assumed pore geometry. Only if the pore saturation is known can the free pore space be calculated, which then determines the Knudsen number. In **Figure 3**, the pore saturation is shown for three different relative humidities of $RH = 0.2, 0.6,$ and 0.95 for the three pore geometries shown in Figure 2. It is the case for all pore geometries that the lower the relative humidity, the lower is the pore saturation. Furthermore, Figure 3 shows that the slit pore has the lowest saturation. In comparison, the cylindrical

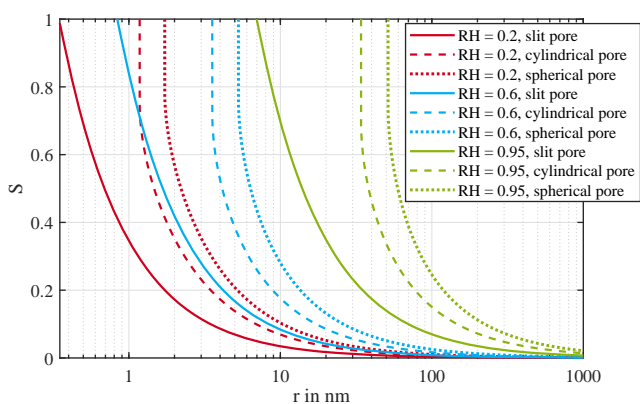


Figure 3. Pore saturation of a slit, cylindrical, and spherical pore geometry at three humidity levels.

pore shows a significantly higher pore saturation, which is caused by the curvature of the adsorbed water layer in one direction. In case of a spherical pore, a water layer curvature in two perpendicular directions is present. Therefore, spherical pores always show the highest saturation for a certain humidity level as shown in Figure 3. The smaller the pore size, the greater is the variation between the pore geometries. In contrast, at large pore radii above $1 \mu\text{m}$, the influence of pore geometry becomes negligible, even for the high humidity of $RH = 0.95$.

3.2. Investigated Pore Size Distributions

Pore saturation can be calculated for a pore of any radius.^[45,48] However, materials have more than just one pore radius. In general, hydraulically bound materials have a pore size distribution of between $r = 1 \text{ nm}$ and 0.1 mm . However, the influence of pore saturation is reduced in pores above $r = 100 \text{ nm}$. Three theoretical pore size distributions are therefore assumed for further analysis, having normal distributions with a varying mean radius μ_r and a standard deviation σ_r . The ratio σ_r/μ_r is constant at 0.2, as shown in **Table 1**. These narrow, unimodal pore size distributions are used to quantify the influence of saturation and pore geometry on the Knudsen effect. The integral of every pore distribution is set to 1. This general formulation may help to make the results applicable to any other material with nanopores as well.

The smallest radius in the computation is $r_{\text{min}} = 0.175 \text{ nm}$, with the maximum being $r_{\text{max}} = 1 \mu\text{m}$. Starting with the smallest radius, the radius at every further sampling point r_{i+1} is increased by 0.1%, as shown in Equation (10). This approach leads to a total of 8657 sampling points.

$$r_{i+1} = r_i \times 1.001 \quad (10)$$

In addition to the theoretical distributions, the real pore volume distributions of a UHPC were investigated. The mixture is mainly based on the cement “CEM I 42.5 Dyckerhoff weiß” with some additives. Furthermore, a superplasticizer based on polycarboxylate was added. The formula used leads to a water–cement ratio of 0.26 and a water–binder ratio of 0.223.^[49,50] The manufactured self-compacting concrete slabs were stored in a box with high humidity for 1 day. The formwork was then stripped off and a posttreatment started. One slab was stored for 6 days in a water basin at 23°C . The resulting compressive strength was $f_c = 85 \text{ N mm}^{-2}$. The second slab being investigated was autoclaved for 8 h at 200°C and 15 bar water vapor saturation pressure. The final compressive strength was $f_c = 150 \text{ N mm}^{-2}$. Both concrete slabs had a bulk density of around 2.3 g cm^{-3} .^[51]

These pore distributions are based on a combination of mercury intrusion porosimetry and gas adsorption.^[52,53] The mercury intrusion porosimetry generates test pressures of

Table 1. Investigated normal-distributed pore size distributions.

Distribution	N_{r_2}	$N_{r_{10}}$	$N_{r_{50}}$
Mean radius	$\mu_r = 2 \text{ nm}$	$\mu_r = 10 \text{ nm}$	$\mu_r = 50 \text{ nm}$
Standard deviation	$\sigma_r = 0.4 \text{ nm}$	$\sigma_r = 2 \text{ nm}$	$\sigma_r = 10 \text{ nm}$

between 0.02 and 400 MPa. The conversion from pressure to a certain pore radius includes the Washburn equation.^[54] The measurement procedure used is an exact reproduction of the international standard.^[52] The calculated pore radius starts at $\approx 100 \mu\text{m}$ and sensitivity is recorded down to a minimum pore radius of $\approx 2 \text{ nm}$. The model assumes cylindrical pores when converting pressure into pore sizes. The other method used is gas adsorption^[53,55] based on the physisorption of nitrogen gas at 77 K in a pressure range of 4.5 mbar to 1 bar. The conversion from pressure to a certain pore diameter is based on the Barrett–Joyner–Halenda (BJH) theory.^[56] The BJH theory includes the layer thickness of the adsorbed nitrogen according to Halsey^[57] and the Kelvin equation for calculating the pore radius. The measurement procedure used is an exact reproduction of the international standard.^[55] The measured pore radii ranged between 0.8 and 100 nm. To capture the entire pore volume distribution, the mercury intrusion data between 100 μm and 2 nm were completed by the gas sorption data from 2 to 0.8 nm.^[58] The porosity of the UHPC slab in the water basin was 7.04% and the autoclaved UHPC had a porosity of 11.1%.

3.3. Material Parameters

Table 2 recapitulates the parameters to compute the pore saturation. All parameters are defined for a standard ambient pressure of $p = 101325 \text{ Pa}$ and an ambient temperature of $T = 296.15 \text{ K}$.

With the air density ρ_{air} in kg m^{-3} and the numerical constant u , l_m amounts to $l_{m,\text{H}_2\text{O}} = \sqrt{\frac{\pi}{8}} \frac{\eta}{u \sqrt{p \rho_{\text{air}}}} = 66.35 \times 10^{-9} \text{ m}$.^[59] C is adapted to cement-based materials.^[14]

4. Results

First, the Knudsen effect and its dependency on pore saturation are discussed for cylindrical pores. The evolution of the Knudsen quotient is then compared for all three pore geometries and all humidity levels. Based on this quantification for single pores, entire pore volume distributions are considered, both theoretical distributions and the measured distributions of an UHPC. This shows the reduction of molecular gas diffusion due to the partial saturation of the material.

Table 2. Material parameters and properties used for free liquid water and water vapor at 296.15 K and 101 325 Pa.

Parameter	Numeric value	Unit
C	15	
M	180153×10^{-6}	kg mol^{-1}
R	8.314	$\text{J mol}^{-1} \text{K}^{-1}$
γ	72232×10^{-6}	N m^{-1}
η	18.381×10^{-6}	Pas
ρ_{air}	1.19221	kg m^{-3}
u	0.49874	
$p_{v,\text{sat}}$	2815.7	Pa

4.1. The Knudsen effect in Partially Saturated Cylindrical Pores

In a first step, the Knudsen quotient in Equation (8) was calculated for cylindrical pores, probably the most popular pore geometry. Obviously, the maximum possible free space can be found in a dry pore. In the following, dry is defined as pores without any layer of water or adsorbed water molecules. Nevertheless, the confinement of dry pores already reduces the molecular diffusion. The Knudsen quotient is 0.97 for a dry, cylindrical pore of $r = 1 \mu\text{m}$ as shown in **Figure 4**. Thus, the molecular diffusion is already reduced by 3% due to the Knudsen effect. If the pore radius is reduced further, the Knudsen effect will be stronger. A reduction of 50% is reached for a dry pore of $r = 33.2 \text{ nm}$. And at a pore radius of 1 nm, the Knudsen number of water vapor is $N_{\text{K,H}_2\text{O}} = 33$ and the Knudsen quotient amounts to 3%. At such small pore radii, Knudsen diffusion dominates and molecular diffusion becomes insignificant.

When the cylindrical pore starts to adsorb water, a water layer is formed at the pore fringe. This reduces the available pore space and, consequently, the Knudsen quotient as shown in **Figure 4**. As humidity levels increase, pores become fully saturated and the Knudsen quotient goes down to zero. At $r = 1 \mu\text{m}$, the influence of pore saturation is negligible for all humidity levels. For a high humidity of $\text{RH} = 0.95$, the effect of pore saturation on the Knudsen quotient is still negligible for pores larger than $r = 100 \text{ nm}$. In contrast, low humidity levels of $\text{RH} \leq 0.4$ significantly reduce the Knudsen quotient at pore radii of $r \leq 5 \text{ nm}$. Thus, the smaller the pore, the greater is the influence of partial saturation on the effective gas diffusion.

4.2. The Knudsen Effect in Various Pore Geometries

For pore radii below 100 nm, the pore saturation starts to reduce the Knudsen quotient significantly. Different pore geometries have different sorption behavior. In comparison with cylindrical pores, slit pores saturate later and spherical pores earlier. The resulting Knudsen quotient is shown for three humidity levels in **Figure 5**. At $\text{RH} = 0.2$, the adsorbed water layer is less than 0.5 nm.^[45] Thus, the three pore geometries show very similar Knudsen quotients. At radii below 2 nm, the critical radius for

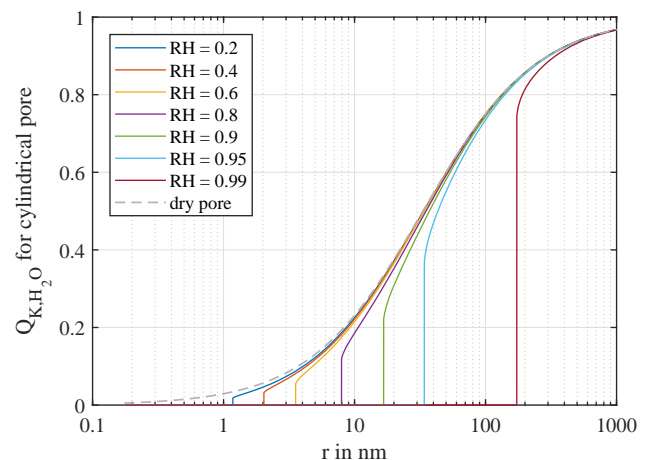


Figure 4. Knudsen quotient of water vapor in cylindrical pores.

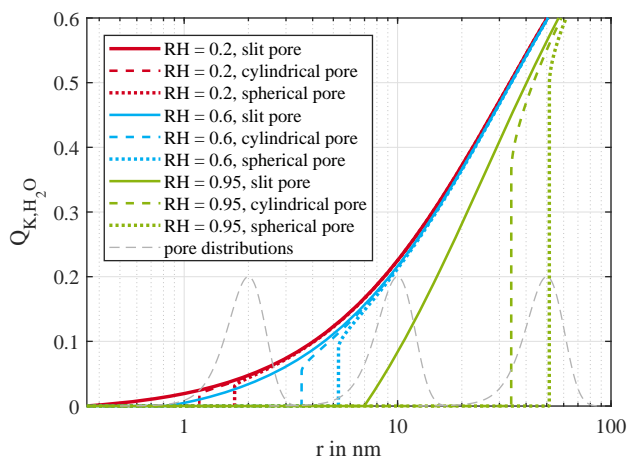


Figure 5. Knudsen quotient for different pore geometries at three humidity levels.

the spherical and cylindrical pores is reached, and pores are fully saturated. At $RH = 0.6$, the Knudsen quotient varies slightly between the different pore geometries for $r \leq 10$ nm. Nevertheless, the full saturation of pores at the critical radius has a great impact on the results. At a humidity of $RH = 0.6$, spherical pores have a critical radius of $r_c = 5.3$ nm, cylindrical pores of $r_c = 3.8$ nm, and slit pores of $r_c = 0.8$ nm. Furthermore, Figure 5 shows the three normally distributed pore sizes qualitatively. As shown, if cylindrical or spherical pores are assumed for the pore distribution N_{r_2} , all pores are already fully saturated. Only slit pores would remain partially saturated, which would enable gas diffusion. At $RH = 0.95$, all slit pores below 7 nm are fully saturated. The critical radius of the spherical and cylindrical pore is around 40 nm. This clearly shows that the influence of pore geometry on the Knudsen quotient can be huge for certain pore volume distributions.

4.3. Reduction of the Molecular Diffusion due to the Knudsen Effect

The Knudsen quotient is determined for different pore geometries and humidity levels. The integration of the Knudsen number over the given pore size distribution yields the water vapor flux according to Equation (1). This equation includes several material parameters, e.g., the molecular diffusion of the considered gas. In the following, the normalized effective gas diffusion coefficient in Equation (9) is considered for better comparison. $D_{\text{eff, norm}}$ depends only on the pore geometry, the pore volume distribution, and the saturation. Thus, it quantifies directly the influence of the Knudsen effect on molecular diffusion.

Three approaches will be compared using this method. First, dry pores are assumed for all humidity levels. This gives the maximum diffusion. In a second approach, the critical radius and pore saturation are predicted, and the Knudsen quotient is calculated. This is the most precise approach but also requires the greatest computational effort. The third approach assumes that the pores of the system are either completely dry or fully saturated. For this, only the critical radius needs to be known.

This kind of binary pore state is often used in capillary bundle models.^[60–63] This simplified model is more precise than the model assuming dry pores at all humidity levels, but the computational costs are negligible.

Figure 6 shows the computed normalized effective gas diffusion coefficient, assuming equally distributed pore sizes between $0.175 \text{ nm} \leq r \leq 1 \mu\text{m}$. This is comparable to Figure 4. If all pores are dry, Figure 6 shows that the normalized effective gas diffusion coefficient of the pore distribution will be 0.89. This means that the confinement of the pore walls already reduces the molecular diffusion. The effective gas diffusion is 11% lower than pure molecular diffusion. The other lines in Figure 6 show the normalized effective gas diffusion for the three pore geometries. The solid lines illustrate the precise model, which includes the critical radius and pore saturation. The dashed lines represent the simplified model, which only considers the critical radius. For $RH \leq 0.8$ in Figure 6, neither pore geometry nor pore saturation has an influence. For higher humidity, the spherical pore shows the strongest trend. In contrast, the slit pore is in good agreement with the dry pore model, even at a high humidity of $RH \approx 0.95$. At a high humidity of $RH \geq 0.85$, the moisture flux is already dominated by hydraulic conductivity and water vapor diffusion becomes negligible.^[64] Thus, for such a broad pore distribution, the influence of pore geometry and pore saturation can be disregarded for moisture flux predictions. In contrast, other gases such as N_2 and CO_2 still migrate well through the pore system at these high levels of water adsorption. In this case, it might be important to take the Knudsen effect into account for gas diffusion prediction.

Although the Knudsen effect of partially saturated pores is negligible for broad pore distributions, narrow unimodal pore distributions might be significantly influenced, as shown in Figure 5. Pore sizes in the lower nanometre range typically dominate in hydraulically bound materials, especially in high-performance concrete. Here, most pores are around 50 nm or even lower.^[11,12] To investigate this, the Knudsen effect is computed again, this time for normally distributed pore sizes with a mean radius of 2 nm.

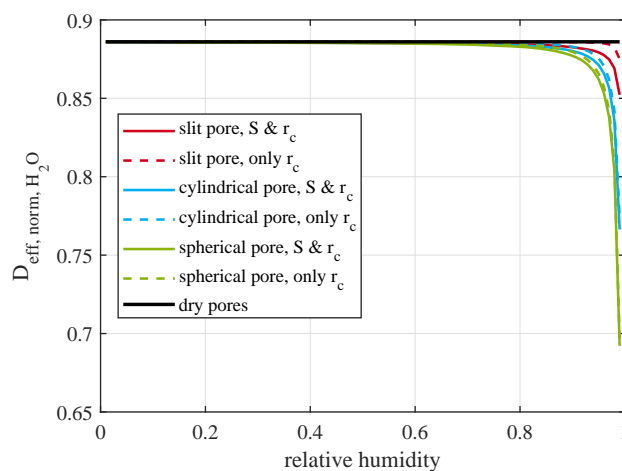


Figure 6. Normalized effective gas diffusion coefficient for equal distributed pore sizes of $0.175 \text{ nm} \leq r \leq 1 \mu\text{m}$.

If the pore system is assumed to be completely dry, the effective normalized gas diffusion will be 0.055, as shown in **Figure 7**. Thus, the molecular diffusion is already remarkably reduced due to the pore confinement. If water adsorption occurs, the pore geometry also has a strong influence. In the case of a spherical pore, almost all pores are fully saturated at around $RH = 0.4$ and gas diffusion goes down to zero. However, at a low humidity level of $RH = 0.22$, the gas diffusion is already reduced by 50% due to the adsorbed water layer. A similar trend can be observed for cylindrical pores, although at slightly higher humidity levels. If only the critical radius is considered and the partial saturation is ignored, the molecular diffusion is reduced as well. This alone would lead to a better prediction of gas diffusion, although the correlation with the precise model is poor. If a slit pore geometry is assumed, the trend is quite different compared to the other two geometries. Here, the descent of the effective gas diffusion covers a broad humidity range and is reaching zero at around $RH = 0.85$. The simplified model shows no effect below $RH = 0.65$. Thus, only the precise models lead to reliable diffusion rates for slit pores. The molecular diffusion is drastically reduced due to the small pores. Nevertheless, pore saturation and pore geometry still have a remarkable effect on gas diffusion. For service life predictions, these effects must be taken into account if such small pores dominate the pore distribution.

In **Figure 8**, $D_{\text{eff, norm}}$ is shown for a pore distribution with a mean radius of 10 nm. If all pores are assumed to be dry, the quotient is 0.22. Thus, the effective gas diffusion coefficient is four times higher than that of the previous examples, which used a radius of 2 nm. However, pores with a radius of 10 nm show a transient regime of diffusion mechanisms, with Knudsen diffusion and molecular diffusion coexisting. Up to a humidity of $RH = 50\%$, diffusion is only reduced by 10% due to pore saturation, independent of the pore geometry. If the humidity is increased further, the spherical pore and the cylindrical pore show a significant decrease at around $RH = 70\%$. Furthermore, the approach that only considers the critical radius correlates well with the precise model. In contrast, the slit pore geometry only has an effect at a high humidity and the

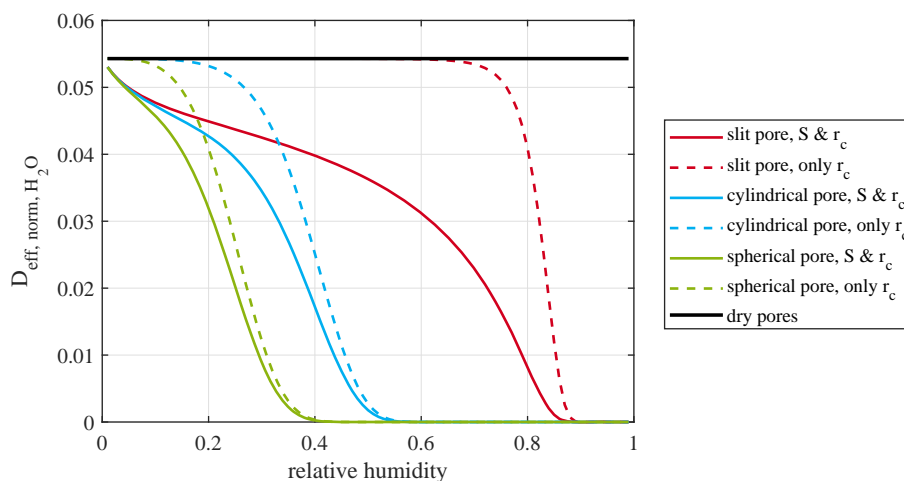


Figure 7. Normalized effective gas diffusion coefficient for normal distributed pore sizes with $\mu_r = 2$ nm and $\sigma_r = 0.4$ nm.

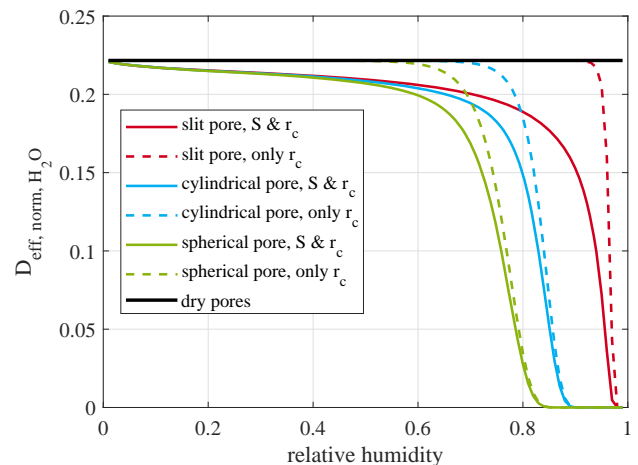


Figure 8. Normalized effective gas diffusion coefficient for normal distributed pore sizes with $\mu_r = 10$ nm and $\sigma_r = 2$ nm.

correlation between the two approaches is weak. Nevertheless, in this transient diffusion regime, the pore saturation has a remarkable influence on the effective gas diffusion.

The third pore distribution investigated, with a mean radius of 50 nm, is analyzed in **Figure 9**. When only the pore geometry is considered, $D_{\text{eff, norm}}$ will be 0.58. Thus, diffusion still occurs in the transient regime, although molecular diffusion becomes more pronounced. Up to a humidity of $RH = 85\%$, the effect of pore saturation can be disregarded. However, above this humidity level, the influence of the pore saturation goes up. For the spherical and cylindrical pore, the correlation between the two approaches is high. The overall trend for the normal distribution with $\mu_r = 50$ nm in **Figure 9** and the equal distribution over the broad range of 0.175 nm $\leq r \leq 1$ μ m in **Figure 6** are very similar.

Based on these three narrow pore distributions, it is shown that pore sizes and pore geometry have a significant influence on diffusion in porous media.

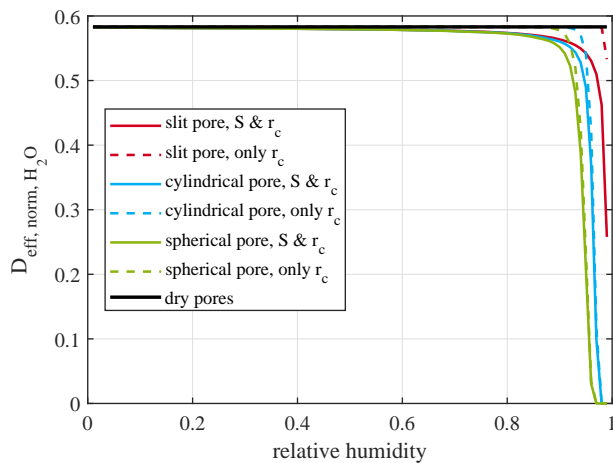


Figure 9. Normalized effective gas diffusion coefficient for normal distributed pore sizes with $\mu_r = 50$ nm and $\sigma_r = 10$ nm.

4.4. Reduction of the Effective Gas Diffusion due to the Knudsen Effect in UHPC

Strictly equally distributed and narrow normally distributed pore sizes do not represent the real pore size distributions; they are theoretical values that cannot be used to develop a realistic computational model of most porous materials. Thus, in a final step, the Knudsen effect of partially saturated pores is computed based on the measured pore distributions of a common UHPC. This material is a suitable candidate to represent an amorphous material with a broad pore size distribution with a large amount of pore sizes in the lower nanometre range. The UHPC mixture was the same for the two investigated samples, whereas the subsequent curing conditions differed. One sample was stored in a water basin, the other in an autoclave. The two normalized pore size distributions are shown in **Figure 10**. Most pores are between $r = 2$ nm and around 30 nm for the UHPC stored in the water basin with $f_c = 85$ N m⁻². In contrast, the autoclaved

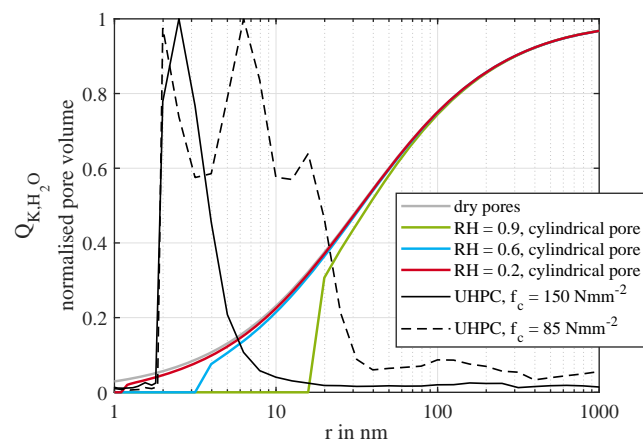


Figure 10. The Knudsen quotient of the UHPC with cylindrical pores at three humidity levels.

UHPC with $f_c = 150$ N m⁻² has a unimodal peak pore at $r = 3$ nm and is significantly narrower. The Knudsen quotient for cylindrical pores is also shown in **Figure 10**. For a humidity of 0.2, the quotient of the partial saturation is close to that of dry pores and the critical radius is significantly below 2 nm. At RH = 0.6, almost all the autoclaved UHPC's pores are affected by the pore saturation. At a high humidity of 0.9, both distributions are almost completely influenced by the partial saturation of the pores.

To compute the effective gas diffusion of the material, the Knudsen quotient of a certain radius is multiplied by the corresponding pore volume. The results of the water-stored UHPC are shown in **Figure 11**. If a dry pore system is assumed, molecular diffusion is already reduced by more than 70% due to the Knudsen effect. The stepwise trend of the lines is the result of the low resolution of the pore radius of mercury intrusion porosimetry and gas adsorption measurement. However, for humidity below 0.2, the pore geometry and saturation have almost no effect. The gas diffusion is reduced by another 10% at RH = 0.5 for spherical pores and at RH = 0.7 for cylindrical pores. Furthermore, the correlation of the precise model and consideration of only the critical radius is high for the spherical and cylindrical pore. At a humidity of above 0.8, the influence of pore saturation on the Knudsen effect becomes significant for all three pore geometries.

The effective gas diffusion of the autoclaved UHPC is shown in **Figure 12**. The reduction in molecular diffusion is more than 80% in dry pores. At a humidity of 0.5, the gas diffusion is further reduced by almost 35% for spherical pores and by more than 20% for cylindrical pores. At RH = 0.9, the effective gas diffusion is almost halved for both pore geometries due to pore saturation. Again, the correlation between the precise model with high computational effort and the model considering only the critical radius and having low computational costs is sufficient. The results for the UHPC with several pores in the lower nanometer range clearly show that the saturation of pores remarkably increases the Knudsen effect and significantly reduces the gas diffusion.

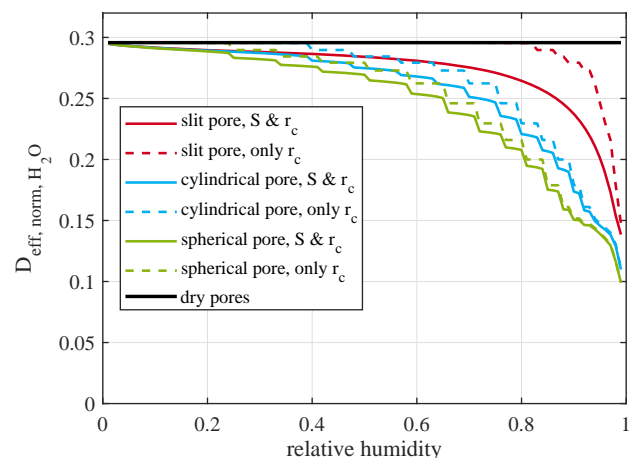


Figure 11. Normalized effective gas diffusion coefficient of the water-stored UHPC with $f_c = 85$ N m⁻².

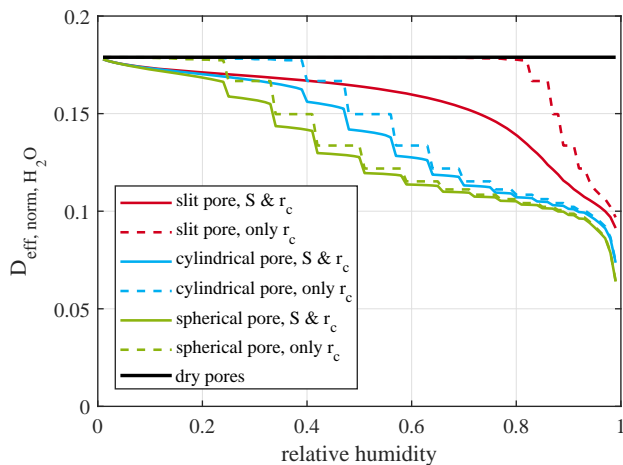


Figure 12. Normalized effective gas diffusion coefficient of the autoclaved UHPC with $f_c = 150 \text{ N mm}^{-2}$.

5. Conclusion

The effective gas diffusion coefficient under consideration of the Knudsen effect and its dependence on pore saturation was quantitatively analyzed. In case of dry pores, the confinement of a pore with a radius of $1 \mu\text{m}$ leads to a reduction of 3% of the effective diffusion, and to a reduction of 25% for a radius of 100 nm. This effect gets more pronounced the smaller the pore radius is. The water layer thickness of partially saturated pores has no significant influence for pore radii above 300 nm at all moisture levels. In contrast, in case of pores of a radius of 2 nm, the influence of the water layer thickness is remarkable already at almost dry conditions corresponding to a relative humidity below 10% RH. In consequence, if porous materials with a significant amount of pores in the lower nanometer range are hydrophilic, the water layer thickness must be considered at any moisture level. The effective gas diffusion is highly influenced. The assumption of just considering the dry pore system to predict the effective gas diffusion would lead to remarkable deviations.

The calculation of the water layer thickness for all pore radii and humidity levels involves high computational effort. To avoid this, a simplified model is presented. This model shows good correlation with the precise model for cylindrical and spherical pores, while the computational costs are negligible. Thus, this simplified model is already a great improvement compared to those models that completely ignore the effect of pore saturation on the effective gas diffusion.

As shown, at high humidity and/or small pore radii below 50 nm, pore saturation has a great influence on the effective gas diffusion due to the Knudsen effect. This should in future be taken into account in computer simulations allowing a prediction of gas transport and an evaluation of the material's performance or degradation. In consideration to the latest developments in nanomaterials, this study might help to estimate the effective gas diffusion of partially saturated pores.

Acknowledgements

The author is grateful to Christian Lehmann (TU Berlin) and Patrick Fontana (R.I.S.E) for providing the UHPC test samples and to Carsten Prinz (BAM, 6.3) for measuring the pore volume distributions.

Open access funding enabled and organized by Projekt DEAL.

Conflict of Interest

The author declares no conflict of interest.

Data Availability Statement

Data sharing is not applicable to this article as no new data were created or analyzed in this study.

Keywords

effective gas diffusion coefficient, gas transport in porous media, knudsen diffusion, moisture transport, nanopores

Received: January 27, 2021

Revised: April 20, 2021

Published online:

- [1] P. Levitz, *J. Phys. Chem.* **1993**, *97*, 3813.
- [2] J. Sekuli_C, J. E. ten Elshof, D. A. Blank, *Adv. Mater.* **2004**, *16*, 1546.
- [3] X. Jin, T. Foller, X. Wen, M. B. Ghasemian, F. Wang, M. Zhang, H. Bustamante, V. Sahajwalla, P. Kumar, H. Kim, G.-H. Lee, K. Kalantar-Zadeh, R. Joshi, *Adv. Mater.* **2020**, *32*, 1907580.
- [4] P. Xu, S. Qiu, J. Cai, C. Li, H. Liu, *J. Power Sources* **2017**, *362*, 73.
- [5] T. Liang, Q. Li, *J. Appl. Phys.* **2019**, *126*, 084304.
- [6] A. M. Odeh, W. Abu-El-Sha'r, R. Al-Ruzouq, *Build. Environment* **2006**, *41*, 492.
- [7] N. Bui, E. R. Meshot, S. Kim, *Adv. Mater.* **2016**, *28*, 5871.
- [8] C. Li, S. M. Meckler, Z. P. Smith, J. E. Bachman, L. Maserati, J. R. Long, B. A. Helms, *Adv. Mater.* **2018**, *30*, 1704953.
- [9] D. W. Hobbs, *Int. Mater. Rev.* **2001**, *46*, 117.
- [10] D. Mu, Z.-S. Liu, C. Huang, N. Djilali, *Microuidics and Nanouidics*, **2008**, *4*(3), 257.
- [11] F. Gong, D. Zhang, E. Sicut, T. Ueda, *J. Mater. Civ. Eng.* **2014**, *26*, 1.
- [12] R. A. Cook, K. C. Hover, *Cem. Concr. Res.* **1999**, *29*, 933.
- [13] J. Sercombe, R. Vidal, C. Gallé, F. Adenot, *Cem. Concr. Res.* **2007**, *37*, 579.
- [14] Y. Xi, Z. P. Bažant, L. Molina, H. M. Jennings, *Adv. Cem. Based Mater.* **1994**, *1*, 258.
- [15] A. Abbas, M. Carcasses, J.-P. Ollivier, *Mater. Struct.* **1999**, *32*, 3.
- [16] C. Liu, Z. Liu, Y. Zhang, *Cem. Concr. Res.* **2020**, *131*, 106035.
- [17] J.-F. Daian, *Transport in Porous Media* **1988**, *3*, 563.
- [18] G. J. Gluth, W. Zhang, M. Gaggli, B. Hillemeier, F. Behrendt, *Cem. Concr. Res.* **2012**, *42*, 656.
- [19] M. Boumaaza, B. Huet, G. Pham, P. Turcry, A. Ait-Mokhtar, C. Gehlen, *Mater. Struct.* **2018**, *51*, 51.
- [20] V. Dutzer, W. Dridi, S. Poyet, P. Le Bescop, X. Bourbon, *Cem. Concr. Res.* **2019**, *123*, 105795.
- [21] Z. Zhang, M. Thiery, V. Baroghel-Bouny, *Cem. Concr. Res.* **2016**, *89*, 257.
- [22] B. K. Nyame, J. M. Illston, *Mag. Concr. Res.* **1981**, *33*, 139.
- [23] S. A. Reinecke, B. E. Sleep, *Water Resour. Res.* **2002**, *38*, 1.

- [24] H.-W. Song, S.-J. Kwon, K.-J. Byun, C.-K. Park, *Cem. Concr. Res.* **2006**, 36, 979.
- [25] R. Luo, C. Tu, *Mag. Concr. Res.* **2019**, 207, 145.
- [26] X. Lin, Q. Hu, Z. Chen, Q. Wang, T. Zhang, M. Sun, *Vadose Zone J.* **2020**, 19, e20063.
- [27] Y. F. Houst, F. H. Wittmann, *Cem. Concr. Res.* **1994**, 24, 1165.
- [28] R. F. Feldman, P. J. Sereda, *J. Appl. Chem.* **1964**, 14, 87.
- [29] W. Zheng, S. H. Kim, *J. Electrochem. Soc.* **2018**, 165, F468.
- [30] M. Boumaaza, P. Turcry, B. Huet, A. Ait-Mokhtar, *Constr. Build. Mater.* **2020**, 253, 1.
- [31] T. Ishida, K. Maekawa, T. Kishi, *Cem. Concr. Res.* **2007**, 37, 565.
- [32] T. Ishida, K. Maekawa, in: *Proceedings of fib Congress Osaka*, **2002**.
- [33] A. S. Ziarani, R. Aguilera, *Transport in Porous Media* **2012**, 91, 239.
- [34] Y. Guo, X. He, W. Huang, M. Wang, *Transport in Porous Media* **2019**, 126, 431.
- [35] W. Hu, Y. Jiang, D. Chen, Y. Lin, Q. Han, Y. Cui, *Appl. Sci.* **2018**, 8, 2097.
- [36] Z. Li, X. Zhang, Y. Liu, *Geoderma* **2017**, 303, 196.
- [37] T. C. Deepagoda, L. W. De Jonge, K. Kawamoto, T. Komatsu, P. Moldrup, *Vadose Zone Journal* **2015**, 14.
- [38] D. Thorstenson, D. Pollock, *Rev. Geophys.* **1989**, 27, 61.
- [39] M. Collin, A. Rasmuson, *Soil Sci. Soc. Am. J.* **1988**, 52, 1559.
- [40] R. Baker, S. Frydman, *Eng. Geol.* **2009**, 106, 26.
- [41] K. Maekawa, R. Chaube, T. Kishi, *Modelling Of Concrete Performance*, E & FN Spon, London **1999**.
- [42] L. Martinez, F. Florido-Diaz, A. Hernández, P. Prádanos, *J. Membr. Sci.* **2002**, 203, 15.
- [43] T. K. Tokunaga, *Water Resour. Res.* **2009**, 45.
- [44] K. Maekawa, T. Ishida, T. Kishi, *J. Adv. Concr. Technol.* **2003**, 1, 91.
- [45] A. Hillerborg, *Cem. Concr. Res.* **1985**, 15, 809.
- [46] S. Brunauer, P. H. Emmett, E. Teller, *J. Am. Chem. Soc.* **1938**, 60, 309.
- [47] W. Thomson, *The London, Edinburgh, and Dublin Philosophical Magazine and Journal of Science* **1871**, 42, 448.
- [48] C. Strangfeld, S. Kruschwitz, *Constr. Build. Mater.* **2018**, 177, 511.
- [49] C. Lehmann, Master's thesis, Technische Universität Berlin **2008**.
- [50] C. Lehmann, P. Fontana, U. Müller, in *Nanotechnology in Construction* Vol. 3, Springer, Berlin Heidelberg **2009**, p. 287.
- [51] P. Fontana, in *Proceedings of Brittle Matrix Composites 9*, Vol. 1, Warsaw, Poland **2009**, p. 391.
- [52] ISO, 15901-1:2016(E): Evaluation of pore size distribution and porosity of solid materials by mercury porosimetry and gas adsorption – Part1: Mercury porosimetry, International Standard **2016**.
- [53] DIN, 66134: 1998-02: Bestimmung der Porengrößenverteilung und der spezifischen Oberfläche mesoporöser Feststoffe durch Stickstoffsorption, Deutsche Norm, German Standard **1998**.
- [54] E. W. Washburn, *Phys. Rev.* **1921**, 17, 273.
- [55] ISO, 15901-2:2006(E): Pore size distribution and porosity of solid materials by mercury porosimetry and gas adsorption - Part 2: Analysis of mesopores and macropores by gas adsorption, International Standard **2006**.
- [56] E. P. Barrett, L. G. Joyner, P. P. Halenda, *J. Am. Chem. Soc.* **1951**, 73, 373.
- [57] G. Halsey, *J. Chem. Phys.* **1948**, 16, 931.
- [58] U. Müller, C. Lehmann, P. Fontana, *Proceedings of 12th Euroseminar on Microscopy Applied to Building Materials*, Dortmund, Germany **2009**, pp. 1–9.
- [59] S. G. Jennings, *J. Aerosol Sci.* **1988**, 19, 159.
- [60] R. F. Feldman, P. J. Sereda, *Matér. Constr.* **1968**, 1, 509.
- [61] M. Lebeau, J.-M. Konrad, *Water Resour. Res.* **2010**, 46.
- [62] B. Pradhan, M. Nagesh, B. Bhattacharjee, *Cem. Concr. Res.* **2005**, 35, 1724.
- [63] M. Edelmann, T. Zibold, J. Grunewald, *Cem. Concr. Res.* **2019**, 119, 126.
- [64] C. Strangfeld, *Constr. Build. Mater.* **2020**, 263, 1.